

Effect of transition-metal substitution in iron-based superconductors

S. L. Liu¹ and Tao Zhou²

¹*College of Science, Nanjing University of Posts and Telecommunications,
Nanjing 210003, China*

²*College of Science, Nanjing University of Aeronautics and Astronautics,
Nanjing 210016, China*

(Dated: November 5, 2018)

We study theoretically the effect of transition-metal (TM) substitution in iron-based superconductors through treating all of the TM ions as randomly distributed impurities. The extra electrons from TM elements are localized at the impurity sites. In the mean time the chemical potential shifts upon substitution. The phase diagram is mapped out and it seems that the TM elements can act as effective dopants. The local density of states (LDOS) is calculated and the bottom becomes V-shaped as the impurity concentration increases. The LDOS at the Fermi energy $\rho(\omega = 0)$ is finite and reaches the minimum at the optimal doping level. Our results are in good agreement with the scanning tunneling microscopy experiments.

PACS numbers: 74.70.Xa, 74.62.En, 74.55.+v

The iron-based superconductors have been studied intensively since their discovery¹. It is widely believed that the main physics in this family of materials is with the iron-arsenic planes. Superconductivity can be realized by doping either holes or electrons into the system.

The transition-metal (TM) elements (such as Co or Ni) are widely used to achieve superconductivity by substituting the iron ions²⁻⁴. However, this substitution is significantly different from other doped materials, namely, the TM ions enter the conducting planes and may also act as the impurities. The competition of the doping effect and impurity effect in the TM-doped materials is of great interest. The scattering effect induced by the impurity has been studied intensively. It has been proposed to account for many unusual physical properties⁵⁻¹⁴. Since it is expected that all of the TM-ions enter the conducting planes, the impurity concentration is expected to equal to the doping density. While so far little attention has been paid to this issue when studying the impurity effect, which may account for some unusual experimental observations of the TM-doped compound.

Recently, the TM substitution effect has attracted broad interest¹⁵⁻¹⁹. For Co(Ni) substitutes, it was reported that the extra electrons are concentrated at the Co or Ni sites based on the first-principle density functional method¹⁵⁻¹⁸. Very recently, based on the X-ray absorption experiment it was also indicated that the electronic occupations for iron sites keep constant as Cobalt density changes in the $\text{BaFe}_{2-2x}\text{Co}_{2x}\text{As}_2$ compound¹⁹. These results lead to the fundamental question, namely, whether the TM substitutes provide doping carriers to the system. On the other hand, the numerical calculation based on the first principle calculation revealed that the Fermi energy shifts upon TM substitution although the extra electrons are localized around the impurity site¹⁶⁻¹⁸. The angle-resolved photoemission spectroscopy (ARPES) experiments on $\text{BaFe}_{2-2x}\text{Co}_{2x}\text{As}_2$ ^{20,21} have indicated the evolution of the Fermi surface with Co-substitution, which also seems to propose that the Cobalt

atoms could be treated as dopants. Thus at this stage the TM substitution effect is non-trivial and rich in physics. Studying this issue theoretically may provide insightful hints to clarify the mechanism of superconductivity.

In this Letter, we study the Cobalt doped material and treat all of the Cobalt ions as the randomly distributed impurities. The order parameters and the Fermi energy are obtained self-consistently based on the two-orbital model and the Bogoliubov-de-Gennes (BdG) equations. The extra electrons are totally located at the impurity sites and the electron filling on Fe site keeps the same upon substitution. In the parent compound, the spin-density-wave (SDW) order is revealed due to the Fermi surface nesting. A rigid shift of the Fermi energy occurs upon substitution, which would break the Fermi surface nesting and suppress the SDW order. As a result, the superconducting (SC) order shows up. These results are qualitatively the same with the previous ones in the clean system²². Thus we suggest that the Cobalt substitutes should be treated as the effective dopants in spite that the extra electrons are localized. The local density of states (LDOS) is also studied and we propose that the disordered impurities are necessary to elucidate some striking features revealed by the scanning tunneling microscopy (STM) experiments.

We start from a two-orbital model including the hopping elements, pairing term, on-site interactions and impurity part^{5,11,22}, expressed by

$$H = H_t + H_\Delta + H_{\text{int}} + H_{\text{imp}}. \quad (1)$$

The hopping term H_t can be expressed by

$$H_t = - \sum_{i\mu j\nu\sigma} (t_{i\mu j\nu} c_{i\mu\sigma}^\dagger c_{j\nu\sigma} + \text{H.c.}) - t_0 \sum_{i\mu\sigma} c_{i\mu\sigma}^\dagger c_{i\mu\sigma}, \quad (2)$$

where i, j are the site indices and $\mu, \nu = 1, 2$ are the orbital indices, and t_0 is the chemical potential. The second term is the pairing term, which reads

$$H_\Delta = \sum_{ij} (\Delta_{i\mu j\nu} c_{i\mu\sigma}^\dagger c_{j\nu\bar{\sigma}}^\dagger + \text{H.c.}). \quad (3)$$

The on-site interaction term H_{int} can be written as^{11,12,22,23}

$$H_{\text{int}} = U \sum_{i\mu\sigma \neq \bar{\sigma}} \langle n_{i\mu\bar{\sigma}} \rangle n_{i\mu\sigma} + U' \sum_{i\mu \neq \nu, \sigma \neq \bar{\sigma}} \langle n_{i\mu\bar{\sigma}} \rangle n_{i\nu\sigma} + (U' - J_H) \sum_{i, \mu \neq \nu, \sigma} \langle n_{i\mu\sigma} \rangle n_{i\nu\sigma}, \quad (4)$$

where $n_{i\mu\sigma}$ is the density operator at the site i and orbital μ . The inter-orbital onsite interaction U' is taken to be $U - 2J_H$.

H_{imp} is the impurity part of the Hamiltonian. For Cobalt substitutes, this term should include the potential scattering and the magnetic part. Here we consider the potential scattering at the Cobalt substitutes, which should play dominant role based on the first-principle calculation¹⁴⁻¹⁹. Then this term is written as,

$$H_{\text{imp}} = \sum_{i_m \mu \sigma} V_s c_{i_m \mu \sigma}^\dagger c_{i_m \mu \sigma}. \quad (5)$$

The Hamiltonian can be diagonalized by solving the BdG equations self-consistently,

$$\sum_j \sum_\nu \begin{pmatrix} H_{i\mu j\nu\sigma} & \Delta_{i\mu j\nu} \\ \Delta_{i\mu j\nu}^* & -H_{i\mu j\nu\bar{\sigma}} \end{pmatrix} \begin{pmatrix} u_{j\nu\sigma}^n \\ v_{j\nu\bar{\sigma}}^n \end{pmatrix} = E_n \begin{pmatrix} u_{i\mu\sigma}^n \\ v_{i\mu\bar{\sigma}}^n \end{pmatrix}, \quad (6)$$

where the Hamiltonian $H_{i\mu j\nu\sigma}$ is expressed by,

$$H_{i\mu j\nu\sigma} = -t_{i\mu j\nu} + [U \langle n_{i\mu\bar{\sigma}} \rangle + (U - 2J_H) \langle n_{i\bar{\mu}\bar{\sigma}} \rangle + (U - 3J_H) \langle n_{i\bar{\mu}\sigma} \rangle + \sum_m V_s \delta_{i, i_m} - t_0] \delta_{ij} \delta_{\mu\nu}. \quad (7)$$

The SC order parameter $\Delta_{i\mu j\nu}$ and the local electron density $\langle n_{i\mu} \rangle$ are obtained self-consistently,

$$\Delta_{i\mu j\nu} = \frac{V_{i\mu j\nu}}{4} \sum_n (u_{i\mu\uparrow}^n v_{j\nu\downarrow}^{n*} + u_{j\nu\uparrow}^n v_{i\mu\downarrow}^{n*}) \tanh\left(\frac{E_n}{2k_B T}\right), \quad (8)$$

$$\langle n_{i\mu} \rangle = \sum_n |u_{i\mu\uparrow}^n|^2 f(E_n) + \sum_n |v_{i\mu\downarrow}^n|^2 [1 - f(E_n)]. \quad (9)$$

Here $f(x)$ is the Fermi distribution function and $V_{i\mu j\nu}$ is the pairing strength.

The LDOS is expressed by

$$\rho_i(\omega) = \sum_{n\mu} [|u_{i\mu\sigma}^n|^2 \delta(E_n - \omega) + |v_{i\mu\bar{\sigma}}^n|^2 \delta(E_n + \omega)], \quad (10)$$

where the delta function $\delta(x)$ has been approximated by $\Gamma/\pi(x^2 + \Gamma^2)$ with the quasiparticle damping $\Gamma = 0.01$.

The hopping constants used in this two-orbital model are expressed as⁵

$$t_{i\mu, i \pm \hat{\alpha} \mu} = t_1 \quad \hat{\alpha} = \hat{x}, \hat{y}, \quad (11)$$

$$t_{i\mu, i \pm (\hat{x} + \hat{y}) \mu} = \frac{1 + (-1)^i t_2}{2} + \frac{1 - (-1)^i t_3}{2}, \quad (12)$$

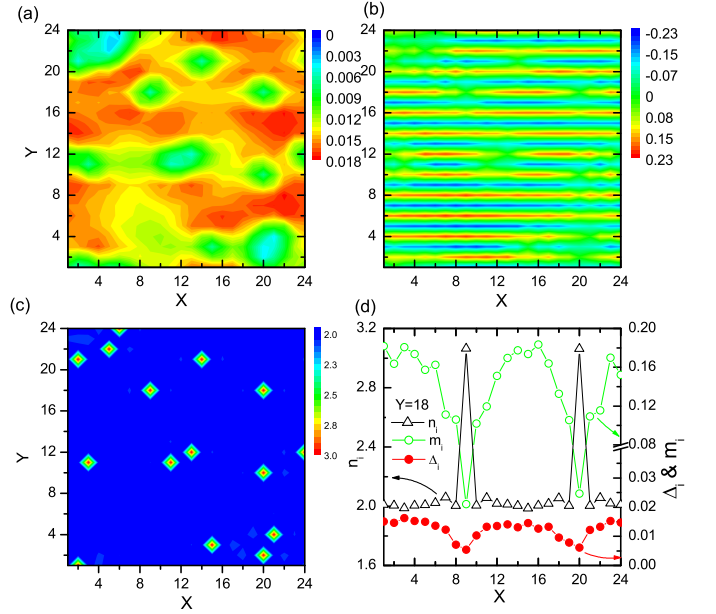


FIG. 1: (Color online) (a-c) The intensity plots of the SC order parameter, magnetic order and particle number with the impurity concentration $x = 0.03$, respectively. (d) The two dimensional cut of the above parameters along $y = 18$.

$$t_{i\mu, i \pm (\hat{x} - \hat{y}) \mu} = \frac{1 + (-1)^i t_3}{2} + \frac{1 - (-1)^i t_2}{2}, \quad (13)$$

$$t_{i\mu, i \pm \hat{x} \pm \hat{y} \mu} = t_4 \quad \mu \neq \nu. \quad (14)$$

In the following presented results, the hopping constants are chosen to be $t_{1-4} = 1.0, 0.5, -1.8, 0.03$. The chemical potential t_0 is determined by the average electron filling per site $\langle n \rangle$ with $\langle n \rangle = 2 + x$, where x is the impurity concentration. The on-site Coulombic interaction is taken as $U = 3.26$ and Hund coupling $J_H = 1.4$. The pairing is chosen as next-nearest-neighbor (NNN) intraorbital pairing with the pairing strength $V = 1.0$, which will reproduce the s_{\pm} pairing symmetry²⁴⁻²⁷. The numerical calculation is performed on a 24×24 lattice at the periodic boundary conditions. To calculate the LDOS, a 40×40 supercell technique is used.

We plot the spatial distribution of the SC order parameter $\Delta_i = \frac{1}{8} \sum_{\alpha\mu} \Delta_{i\mu, i+\alpha\mu}$, the magnetic order $[M_i = \frac{1}{4} \sum_{\mu} (n_{i\mu\uparrow} - n_{i\mu\downarrow})]$, and the particle number $n_i = \sum_{\mu\sigma} n_{i\mu\sigma}$ with the scattering potential $V_s = -3.5$ in Figs. 1(a)-1(c), respectively. Fig. 1(d) displays the two dimensional cut of all of the parameters. As seen, in presence of impurities, the amplitude of the SC order parameter is not uniform. It is reduced at and around the impurity sites. The magnetic spin order is antiferromagnetic along the y direction and ferromagnetic along the x direction, which is consistent with the $(\pi, 0)/(\pi, \pi)$ SDW in the extended/reduced Brillouin zone. This is qualitatively the same with the previous theoretical calculation^{22,23}. At and around the impurity sites, the magnetic order M_i

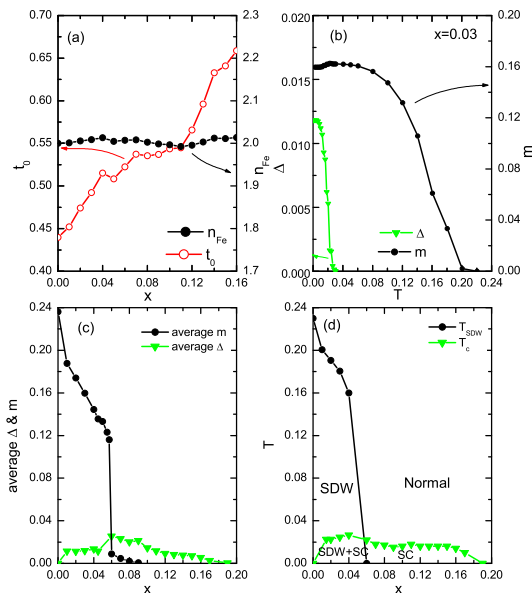


FIG. 2: (Color online) (a) The chemical potential t_0 and the average particle number per Fe ion n_{Fe} as a function of the Cobalt concentration x . (b) The average magnitudes of the SC order parameter Δ and magnetic order M as a function of the temperature with the impurity concentration $x = 0.03$. (c) The average amplitudes of the SC order parameter Δ and the magnetic order M as a function of x . (d) The calculated phase diagram.

is suppressed. The particle number is about 3.0 at the impurity sites and recovers to 2.0 when away from the impurity sites. This result indicates that the electron filling for Fe sites does not change upon Cobalt substitution. This is consistent with the numerical results based on the first principle calculation^{15–18}.

The average electron density per Fe site n_{Fe} and the chemical potential t_0 as a function of the impurity concentration x are plotted in Fig. 2(a). As shown, the electron density is almost unchanged (≈ 2.0) for all of the impurity concentrations we consider, indicating that the extra electrons of impurity atoms are indeed localized around the impurity sites. This is consistent with the first principle calculation^{15–18}. In the mean time, the chemical potential increases monotonically with increasing substitution level x . This result confirms the numerical results based on the first principle calculation^{16–18} and is consistent with the ARPES experiments^{20,21}.

The average amplitudes of the SC order and magnetic order as a function of the temperature and impurity concentration x are shown in Figs. 2(b) and 2(c), respectively. For the fixed impurity concentration $x = 0.03$, as seen in Fig. 2(b), both the magnetic order and the SC order decrease as the temperature increases and two transition temperatures are revealed. At zero temperature, as seen in Fig. 2(c), the magnetic order decreases monotonically with the increasing x and vanishes around $x \simeq 0.06$. The SC order increases as x increases in the low substitution region and reaches its maximum at $x = 0.06$. Then it

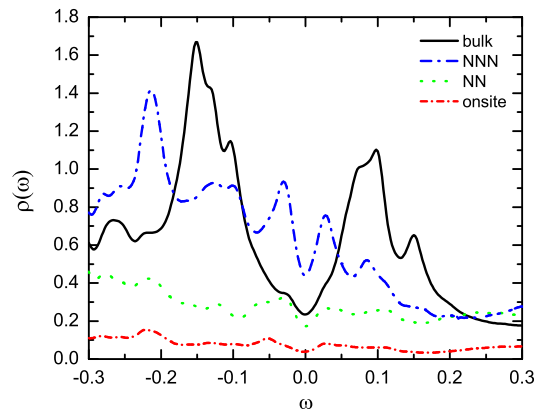


FIG. 3: (Color online) The energy dependent LDOS on the impurity site, NN site and NNN site of the impurity, respectively, with the impurity concentration $x = 0.12$. The solid line represents the LDOS of bulk site which is far away from any impurity.

decreases with further increasing x . The calculated phase diagram is plotted in Fig. 2(d). It can be seen that the magnetic order and SC order coexist in the low impurity concentration region. The magnetic order decreases abruptly at $x = 0.06$, corresponding to the quantum critical point at this concentration. This is well consistent with the experimental results on $\text{BaFe}_{2-2x}\text{Co}_{2x}\text{As}_2$ ^{28,29}. The SC order appears as the magnetic order is suppressed and the SC order reaches the maximum as the magnetic order disappears. All of the obtained results are qualitatively consistent with the previous calculation by merely taking into account the doping effect²².

We have demonstrated that the Fermi energy increases as impurity concentration x increases. The phase diagram and the order parameters as a function of x also indicate that the impurities are indeed act as the effective "dopant", in spite that the electron densities for Fe sites do not change. While the fundamental question still remains about how the TM substitution controls the phase diagram. Actually, for the TM-doped materials, the competition of the SDW and SC orders should play the essential role. The SDW instability originates from the Fermi surface nesting²². It reaches the maximum value for the parent compound due to the perfect nesting at zero doping. The SC order is induced by the spin fluctuation^{25,26} and also relates to the Fermi surface nesting. While for the parent compound the SC order could not survive due to the suppression effect by the SDW order. Both the impurity effect and the shifts of the Fermi energy would suppress the SDW order and then the SC order shows up upon substitution. Actually, here the disorder and the impurities play the important role in this system and to some extent they induce and enhance the SC order through suppressing the SDW order.

We now turn to discuss the LDOS spectra. Shown in Fig. 3 is the LDOS spectra near an impurity with the impurity concentration $x = 0.12$. As seen, the spectra are

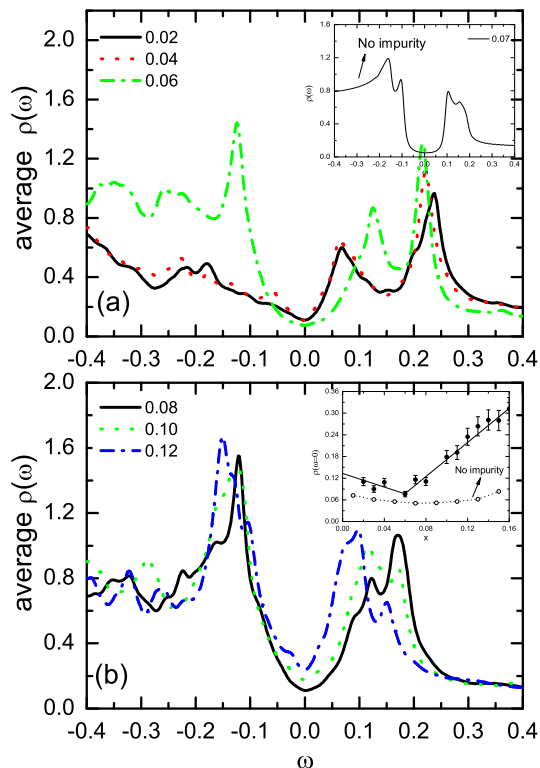


FIG. 4: (Color online) (a) The energy dependent LDOS of $\text{Ba}(\text{Fe}_{1-x}\text{Co}_x)_2\text{As}_2$ superconductor in the low substitution region. Inset: The energy dependent LDOS with doping $x = 0.07$ without impurity. (b) Similar to (a) but in the high substitution region. Inset: The solid circles are the LDOS at the Fermi energy $\rho(\omega = 0)$ versus the impurity concentration x , with the solid lines being guides to the eye. The open circles and dashed line are $\rho(\omega = 0)$ versus the doping density without the impurity.

suppressed at the impurity site and the nearest-neighbor (NN) sites. Two in-gap peaks are clearly seen on the NNN site to the impurity. These results are similar to the previous theoretical results for single-impurity effect¹¹.

Now let us study the LDOS spectra in the bulk which are far away from any impurity site. The average LDOS spectra of four sites are plotted in Figs. 4(a) and 4(b), respectively. The bulk LDOS spectrum without the impurity scattering at the doping level $x = 0.07$ is plotted

in the inset of Fig. 4(a) for a comparison. As seen, for the clean system the LDOS spectrum has a U-shaped bottom, consistent with previous theoretical results²². This is understandable because the SC order parameter is nodeless around the Fermi surface. While interestingly as the impurity concentration increases the bottom becomes V-shaped. This is consistent with the STM experiments on $\text{Ba}(\text{Fe}_{1-x}\text{Co}_x)_2\text{As}_2$ superconductors³⁰⁻³² and the previous theoretical studies based on the T-matrix method⁶. Another interesting feature of the spectrum is the finite value of the LDOS at the Fermi energy [$\rho(\omega = 0)$]. We plot the zero energy LDOS as a function of the impurity concentration in the inset of Fig. 4(b). $\rho(\omega = 0)$ decreases with increasing x and reaches the minimum at the optimal SC sample $x_m = 0.06$. Then it increases with further increasing x . As seen in the inset of Fig. 4(b), $\rho(\omega = 0)$ scales with $|x - x_m|$. This is a striking feature and is well consistent with the STM experiment³². For a comparison we also plot $\rho(\omega = 0)$ as a function of doping density without considering the impurity scattering. As seen, $\rho(\omega = 0)$ is very low and almost doping independent. Our results propose that the impurity effect is essential when explaining some striking features from STM experiments.

In summary, the TM substitution effect in iron-based superconductors is studied by solving the BdG equations self-consistently. We investigate the Cobalt substitutes and the Cobalt atoms are considered as randomly distributed impurities with negative scattering potential. It is shown that the extra electrons are localized around the impurity sites, while the chemical potential increases with the increasing impurity concentration. These results are consistent with the recent first principle calculation and the ARPES experiments. The obtained phase diagram is qualitatively consistent with the previous reports of the $\text{BaFe}_{2-2x}\text{Co}_{2x}\text{As}_2$ superconductors. It is found that the energy dependent LDOS spectrum is V-shaped, and the LDOS at the Fermi energy $\rho(\omega = 0)$ is finite and depends on the impurity concentration. These features are consistent with the STM experiments on $\text{BaFe}_{2-2x}\text{Co}_{2x}\text{As}_2$ material.

We thank S. H. Pan and Ang Li for useful discussion and showing us their STM data before publication. This work is supported by the NSFC under the Grant No. 11004105.

¹ Y. Kamihara et al., J. Am. Chem. Soc. **130**, 3296 (2008).
² A. S. Sefat, R. Jin, M. A. McGuire, B. C. Sales, D. J. Singh, D. Mandrus, Phys. Rev. Lett. **101**, 117004 (2008).
³ Jiun-Haw Chu, James G. Analytis, Chris Kucharczyk, Ian R. Fisher, Phys. Rev. B **79**, 014506 (2009).
⁴ Lei Fang, Huiqian Luo, Peng Cheng, Zhaosheng Wang, Ying Jia, Gang Mu, Bing Shen, I. I. Mazin, Lei Shan, Cong Ren and Hai-Hu Wen, Phys. Rev. B **80**, R140508 (2009).
⁵ Degang Zhang, Phys. Rev. Lett. **103**, 186402 (2009).

⁶ Y. Bang, H. Y. Choi, and H. Won, Phys. Rev. B **79**, 054529 (2009).
⁷ D. Parker, O. V. Dolgov, M. M. Korshunov, A. A. Golubov, and I. I. Mazin, Phys. Rev. B **78**, 134524 (2008).
⁸ A. B. Vorontsov, M. G. Vavilov, and A. V. Chubukov, Phys. Rev. B **79**, R140507 (2009).
⁹ W. F. Tsai, Y. Y. Zhang, C. Fang, and J. P. Hu, Phys. Rev. B **80**, 064513 (2009).
¹⁰ Eugeniu Plamadeala, T. Pereg-Barnea, and Gil Refael, Phys. Rev. B **81**, 134513 (2010).

- ¹¹ Tao Zhou, Huaixiang Huang, Yi Gao, Jian-Xin Zhu, and C. S. Ting, Phys. Rev. B **83**, 214502 (2011).
- ¹² Tao Zhou, Z. D. Wang, Yi Gao, and C. S. Ting, Phys. Rev. B **84**, 174524 (2011).
- ¹³ Hong-Min Jiang, Jia Guo, and Jian-Xin Li, Phys. Rev. B **84**, 014533 (2011).
- ¹⁴ A. F. Kemper, C. Cao, P. J. Hirschfeld, and H.-P. Cheng, Phys. Rev. B **80**, 104511 (2009).
- ¹⁵ H. Wadati, I. Elfimov, and G. A. Sawatzky, Phys. Rev. Lett. **105**, 157004 (2010).
- ¹⁶ K. Nakamura, R. Arita and H. Ikeda, Phys. Rev. B **83**, 144512 (2011).
- ¹⁷ S. Konbu, K. Nakamura, H. Ikeda, and R. Arita, J. Phys. Soc. Jpn. **80**, 123701 (2011).
- ¹⁸ Tom Berlijn, Chia-Hui Lin, William Garber, and Wei Ku, arXiv:1112.4858 (2011).
- ¹⁹ E. M. Bittar, C. Adriano, T. M. Garitezi, P. F. S. Rosa, L. Mendonca-Ferreira, F. Garcia, G. de M. Azevedo, P. G. Pagliuso, and E. Granado, Phys. Rev. Lett. **107**, 267402 (2011).
- ²⁰ Y. Sekiba, T. Sato, K. Nakayama, K. Terashima, P. Richard, J.H. Bowen, H. Ding, Y.-M. Xu, L.J. Li, G.H. Cao, Z.-A. Xu, T. Takahashi, New J. Phys. **11** 025020 (2009).
- ²¹ Chang Liu, A. D. Palczewski, R. S. Dhaka, Takeshi Kondo, R. M. Fernandes, E. D. Mun, H. Hodovanets, A. N. Thaler, J. Schmalian, S. L. Budko, P. C. Canfield, and A. Kaminiski, Phys. Rev. B **84**, R020509 (2011).
- ²² Tao Zhou, Degang Zhang, and C. S. Ting, Phys. Rev. B **81**, 052506 (2010).
- ²³ H.M. Jiang, J.-X. Li, and Z. D. Wang, Phys. Rev. B **80**, 134505 (2009).
- ²⁴ H. Ding, P. Richard, K. Nakayama, T. Sugawara, T. Arakane, Y. Sekiba, A. Takayama, S. Souma, T. Sato, T. Takahashi, Z. Wang, X. Dai, Z. Fang, G. F. Chen, J. L. Luo, and N. L. Wang, Europhys. Lett. **83**, 47001 (2008).
- ²⁵ I. I. Mazin, D. J. Singh, M. D. Johannes, and M. H. Du, Phys. Rev. Lett. **101**, 057003 (2008).
- ²⁶ Zi-Jian Yao, Jian-Xin Li, and Z. D. Wang, New J. Phys. **11**, 025009 (2009).
- ²⁷ Fa Wang, Hui Zhai, Ying Ran, Ashvin Vishwanath, and Dung-Hai Lee, Phys. Rev. Lett. **102**, 047005 (2009).
- ²⁸ Y. Laplace, J. Bobroff, F. Rullier-Albenque, D. Colson, and A. Forget, Phys. Rev. B **80**, R140501 (2009).
- ²⁹ C. Lester, Jiun-Haw Chu, J. G. Analytis, T. G. Perring, I. R. Fisher, and S. M. Hayden, Phys. Rev. B **81**, 064505 (2010).
- ³⁰ Yi Yin, M. Zech, T. L. Williams, X. F. Wang, G. Wu, X. H. Chen, and J. E. Hoffman, Phys. Rev. Lett. **102**, 097002 (2009).
- ³¹ M. L. Teague, G. K. Drayna, G. P. Lockhart, P. Cheng, B. Shen, H.-H. Wen, and N.-C. Yeh, Phys. Rev. Lett. **106**, 087004 (2011).
- ³² S. H. Pan and A. Li (private communication).